

Supporting Information

Efficient separation of uranium(VI) from aqueous solution using magnetic Co/Al layered double oxides coated with carbon dots

Yan Wang^{a*}, Yong Zhang^{b*}, Xiaolin Liu^a, Sen Sun^a, Shiyi Qin^a, Jiaqi Huang^a, Bowei Chen^a

^a School of Mathematics and Physics, Mianyang Teachers' College, Mianyang 621000, PR China.

^b State Key Laboratory of Environment-friendly Energy Materials, Sichuan Co-Innovation Center for New Energetic Materials, National Co-innovation Center for Nuclear Waste Disposal and Environmental Safety, Nuclear Waste and Environmental Safety Key Laboratory of Defense, School of National Defence Science & Technology, Southwest University of Science and Technology, Mianyang 621010, China.

*Corresponding author. E-mail: 100494@mtc.edu.cn (Y. Wang), yongpandm@swust.edu.cn (Y. Zhang).

Adsorption kinetic model

Pseudo-first-order kinetic model

The adsorption kinetics of uranium(VI) on MLC was simulated by pseudo-first-order kinetic model, which was used to describe the physisorption behavior.

$$\text{linear: } \ln(q_e - q_t) = \ln q_e - k_1 t \quad (\text{S1})$$

$$\text{non-linear: } q_t = q_e(1 - e^{-k_1 t}) \quad (\text{S2})$$

Pseudo-second-order kinetic model

The pseudo-second-order kinetic model presumed that the rate-limiting step was essentially chemisorption and the mechanism might involve valence forces by sharing or through the exchange of electrons between adsorbate and adsorbent.

$$\text{linear: } \frac{t}{q_t} = \frac{1}{k_2 q_e^2} + \frac{t}{q_e} \quad (\text{S3})$$

$$\text{non-linear: } q_t = \left(\frac{k_2 q_e^2 t}{1 + k_2 q_e t} \right) \quad (\text{S4})$$

Elovich kinetic model

The Elovich kinetic model considered that the rate-controlling step is the diffusion of the target ions and it revealed the behaviors of chemisorption.

$$q_t = \frac{1}{\beta} \ln(1 + \alpha \beta t) \quad (\text{S5})$$

Intraparticle diffusion kinetic model

The intraparticle diffusion kinetic model assumed that the internal diffusion was a velocity-controlled step and the direction of diffusion is random.

$$q_t = k_{ip} t^{0.5} + C_i \quad (\text{S6})$$

Adsorption isotherm model

Langmuir isotherm model

The Langmuir model assumed that monolayer adsorption took place on the homogenous surfaces. It is one of the most widely used isotherms in adsorption.

$$\text{linear: } \frac{C_e}{q_e} = \frac{1}{K_L q_m} + \frac{C_e}{q_m} \quad (\text{S7})$$

$$\text{non-linear: } q_e = \frac{q_m K_L C_e}{1 + K_L C_e} \quad (\text{S8})$$

Freundlich isotherm model

The Freundlich model has been regarded as an empirical equation without physical meaning. In many published papers, the Freundlich isotherm was applied to represent the multilayer adsorption on heterogamous surfaces.

$$\text{linear: } \ln q_e = \ln K_F + \frac{1}{n} \ln C_e \quad (\text{S9})$$

$$\text{non-linear: } q_e = K_F C_e^{\frac{1}{n}} \quad (\text{S10})$$

Sips isotherm model

The Sips model is a hybrid model combining the Langmuir and Freundlich models and it is the most applicable 3-parameter isotherm model for monolayer adsorption. Besides, the Sips model can describe homogeneous or heterogeneous systems.

$$\text{Linear: } \ln\left(\frac{q_e}{q_m - q_e}\right) = \frac{1}{n} \ln C_e + \ln(K_S)^{1/n_S} \quad (\text{S11})$$

$$\text{Non-linear: } q_e = \frac{q_m K_S C_e^{n_S}}{1 + K_S C_e^{n_S}} \quad (\text{S12})$$

Dynamic adsorption model

Thomas model

Thomas model assumes that adsorption equilibrium is best described by Langmuir isotherm model without axial dispersion and the adsorption process follows pseudo second order reversible reaction kinetics.

$$\text{linear: } \ln\left(\frac{C_o}{C_t} - 1\right) = \left(\frac{K_{Th}q_{Th}m}{Q}\right) - K_{Th}C_o t \quad (\text{S13})$$

$$\text{non-linear: } \frac{C_t}{C_o} = \frac{1}{1 + e^{\left(\frac{K_{Th}q_{Th}m}{Q} - K_{Th}C_o t\right)}} \quad (\text{S14})$$

Yoon-Nelson model

Yoon-Nelson model assumes that the rate of decrease in the probability of adsorption of each adsorbate molecule is proportional to the probability of adsorbate adsorption and the adsorbate breakthrough on the adsorbent, and can predict the adsorption capacity and time when the effluent concentration reaches half of the initial concentration during the dynamic adsorption column.

$$\text{linear: } \ln\left(\frac{C_t}{C_o - C_t}\right) = k_{YN} - \tau k_{YN} \quad (\text{S15})$$

$$\text{non-linear: } \frac{C_t}{C_o} = \frac{e^{(tk_{YN} - \tau k_{YN})}}{1 + e^{(tk_{YN} - \tau k_{YN})}} \quad (\text{S16})$$

Table S1. Relevant parameters of Intra-particle diffusion model.

Stages	Parameters	MLC-1	MLC-2	MLC-3
Stage 1	k_{i1} (mg/g·min ^{1/2})	31.67	34.78	27.35
	C	-11.22	-9.66	16.10
	R ²	0.921	0.980	0.957
Stage 2	k_{i2} (mg/g·min ^{1/2})	0.77	1.88	1.59
	C	74.71	83.24	87.22
	R ²	0.289	0.492	0.758

Table S2. Comparison of removal capacity of uranium(VI) by various adsorbents.

Adsorbents	Temperature (K)	pH	q_{\max} (mg/g)	Reference
$\text{Fe}_3\text{O}_4@\text{C}@\text{MnO}_2$	298	5.0	77.71	Dai et al., 2019
AMGO	298	6.0	141.2	Chen et al., 2016
P- Al_2O_3 MSs	298	5.0	316.9	Huang et al., 2018
DI-SNZVI	298	5.0	427.9	Pang et al., 2019
m SiO_2 /PDA	332	5.5	332.3	Bai et al., 2017
Ni-Co LDH _{W-7}	298	6.0	201.1	Guo et al., 2021
LDH@LDC	308	5.0	267.7	Chen et al., 2022
Ca-Mg-Al-LDO ₆₀₀	298	5.0	486.8	Zou et al., 2016
CNFs aerogel	298	5.0	440.6	Wang et al., 2021
MHC-7	293	4.0	105.3	Li et al., 2020
MLC-3	298	5.0	513.9	This work

Table S3. Atomic percent of MLC-3 before and after uranium(VI) adsorption.

Elements	Before adsorption	After adsorption
Co2p	7.37%	4.12%
Al2p	4.16%	5.84%
Fe2p	5.56%	3.36%
C1s	56.29%	52.68%
O1s	26.63%	33.28%
U4f	-	0.73%



Figure S1. Recovery of adsorbents by the external magnetic field.

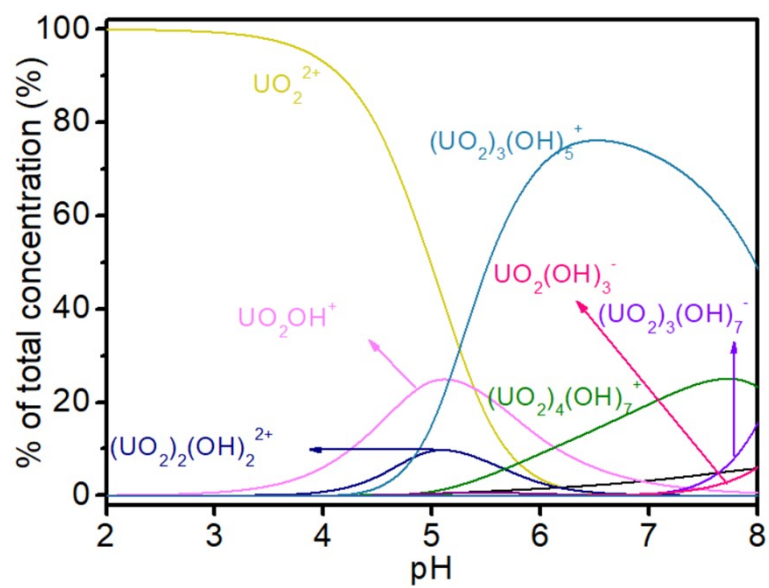


Figure S2. Distribution of uranium(VI) species under different pH.

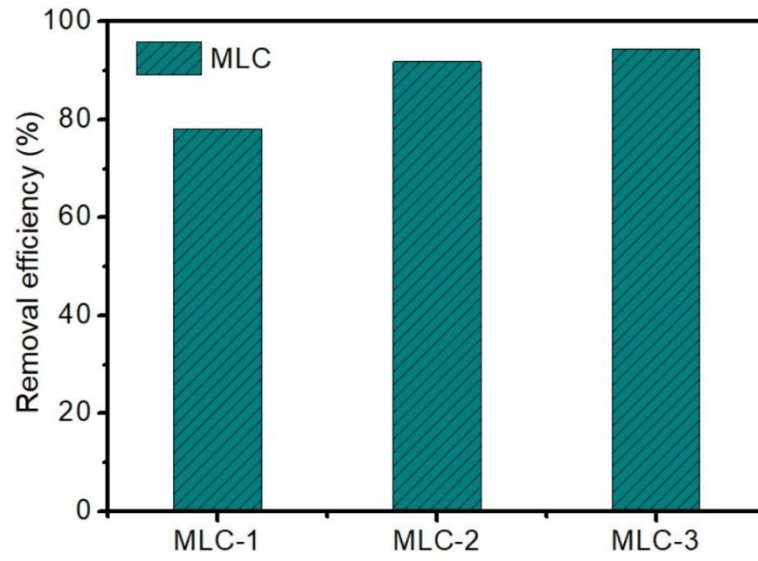


Figure S3. The removal efficiencies of MLC composites ($C_0 = 10$ mg/L, pH = 5.0, T = 298 K, m/V = 0.1 g/L and t = 24 h).

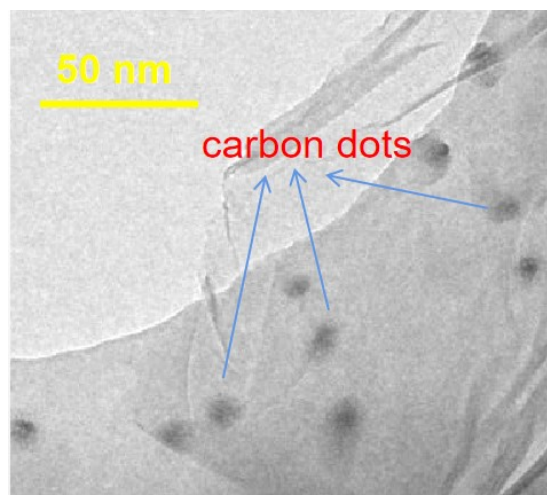


Figure S4. HR-TEM image of MLC-3.

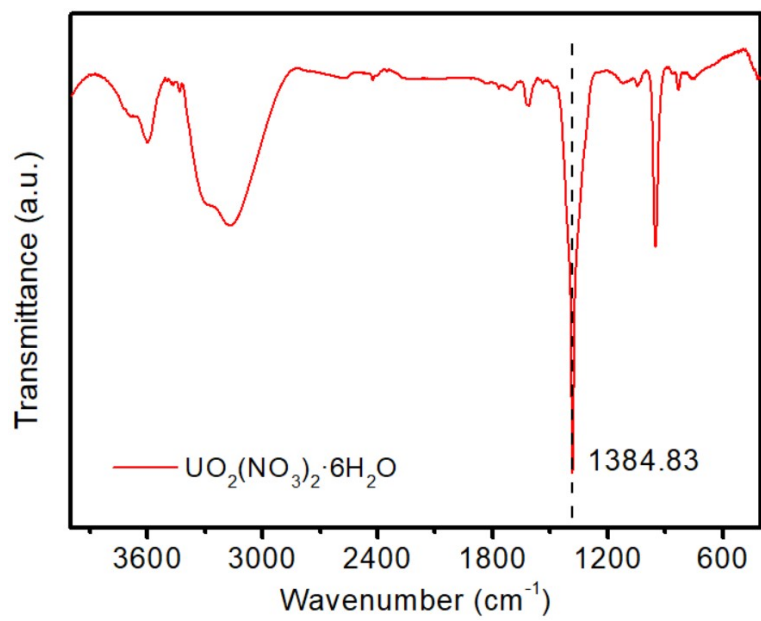


Figure S5. FTIR spectra of $\text{UO}_2(\text{NO}_3)_2 \cdot \text{H}_2\text{O}$.

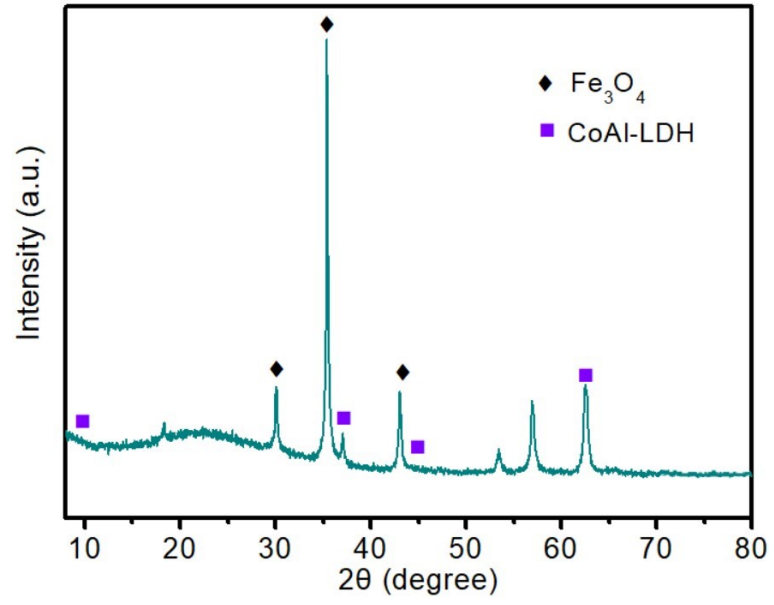


Figure S6. The XRD pattern of of MLC-3 after the cycle test.

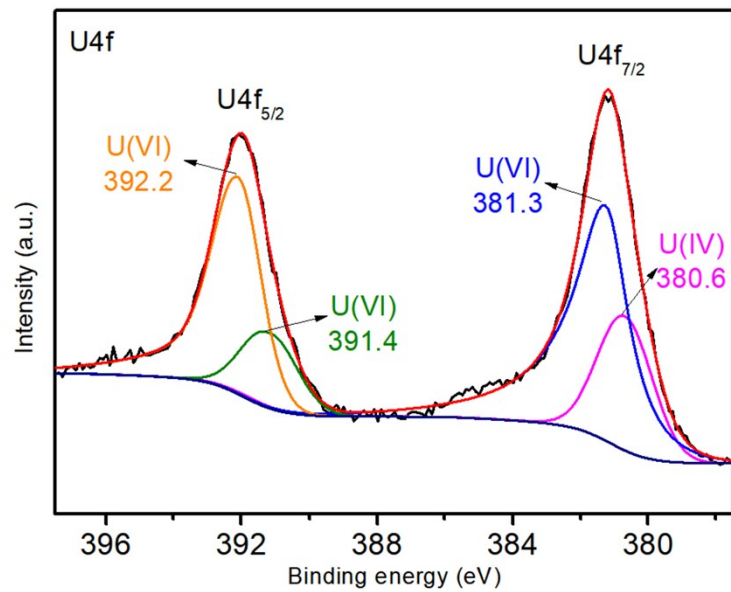


Figure S7. High resolution U4f XPS spectrum of MLC-3 after uranium adsorption.

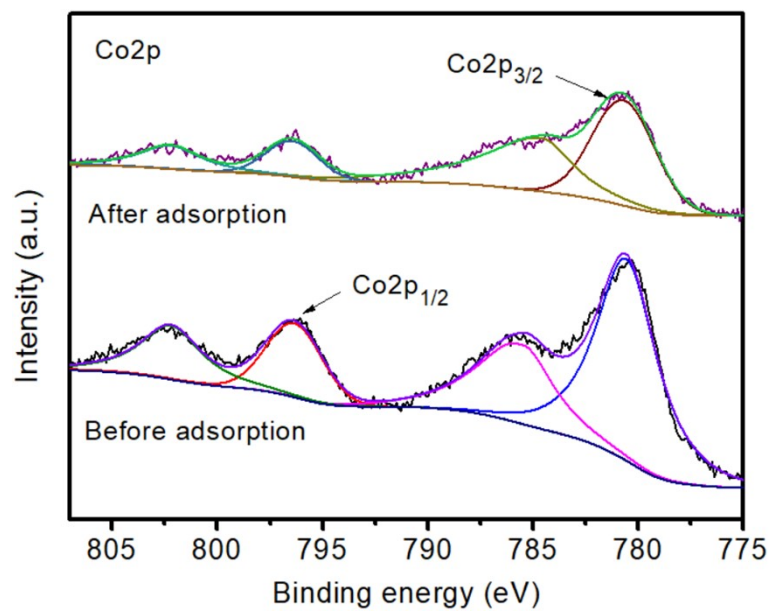


Figure S8. High resolution Co2p XPS spectrum of MLC-3 after uranium adsorption.